THE JOURNAL OF PHYSICAL CHEMISTRY B

ARTICLE

pubs.acs.org/JPCB

Förster Resonance Energy Transfer beyond 10 nm: Exploiting the Triplet State Kinetics of Organic Fluorophores

Heike Hevekerl, Thiemo Spielmann, Andriy Chmyrov,† and Jerker Widengren*

Experimental Biomolecular Physics, Department of Applied Physics, Royal Institute of Technology, Stockholm, Sweden

ABSTRACT: Inter- or intramolecular distances of biomolecules can be studied by Förster resonance energy transfer (FRET). For most FRET methods, the observable range of distances is limited to 1−10 nm, and the labeling efficiency has to be controlled carefully to obtain accurate distance determinations, especially for intensity-based methods. In this study, we exploit the triplet state of the acceptor fluorophore as a FRET readout using fluorescence correlation spectroscopy and transient state monitoring. The influence of donor fluorescence leaking into the acceptor channel is minimized by a novel suppression algorithm for spectral bleed-through, thereby tolerating a high excess (up to 100-fold) of donor-only labeled samples. The suppression algorithm and the high sensitivity of the triplet state to small changes in the fluorophore excitation rate make it possible to extend the observable range of FRET efficiencies by up to 50% in the presence of large donor-only populations. Given this increased range of FRET efficiencies, its compatibility with organic fluorophores, and the low requirements on the labeling efficiency and instrumentation, we foresee that this approach will be attractive for in vitro and in vivo FRET-based spectroscopy and imaging.

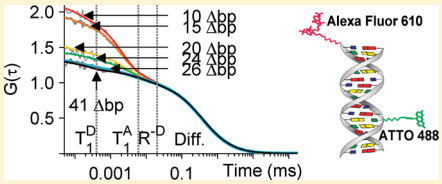

INTRODUCTION

During Förster (or fluorescence) resonance energy transfer (FRET), energy is transferred via a nonradiative dipole−dipole interaction from a donor (D) to an acceptor (A) molecule in a strongly distance-dependent manner. This has made FRET a widely used method to determine inter- or intramolecular distances in the range of typically 1−10 nm.[1] Techniques for FRET estimation can be divided into those applicable to conventional microscopes (intensity-based) and techniques that require dedicated instrumentation (e.g., time-resolved; fluorescence lifetime imaging microscopy (FLIM); single molecule measurements).

The most popular intensity-based approach is steady-state monitoring of the D and A emission upon D excitation.[2−5] Due to the spectral overlap of D and A, the detected A signal is influenced by D emission leaking into the A channel and direct excitation of A. As a result of the spectral bleed-through, additional control measurements have to be acquired of D and A emission for D-only and A-only labeled samples. For most intensity-based approaches, the apparent FRET efficiency can be affected by incompletely labeled FRET pairs, which exist to a substantial amount in most FRET experiments. Therefore, careful calibration measurements are necessary to control the labeling efficiencies and the relative concentrations of D and A.

FLIM is a robust but technically challenging method for FRET estimation.[6] By monitoring changes in the D-fluorescence lifetime, it is immune to spectral bleed-through and A-only labeled samples. FLIM can also differentiate between D-only and D−A labeled samples at high and intermediate FRET efficiencies. At low FRET efficiencies, however, the donor lifetimes of D-only and D−A labeled samples are similar and hence difficult to distinguish. The resulting FRET efficiencies can then be underestimated to a significant degree.

Similar to FLIM, single-molecule multiparameter fluorescence detection (smMFD) has difficulties estimating low FRET efficiencies. To differentiate between fluorescent trajectories of low-FRET species and D-only labeled species, a threshold has to be applied on the detected acceptor signal that often cuts off signals originating from FRET efficiencies <10%. On the other hand, by analyzing multiple parameters (e.g., intensity, lifetime, anisotropy) from individual molecules simultaneously, smMFD can reach a high precision and accuracy in the FRET measurements, identify unspecific quenching effects, and distinguish between D- and/or A-labeled specimen.[7−9]

An alternative method to detect low FRET efficiencies in cell-free systems is luminescence resonance energy transfer (LRET), which uses lanthanides as donors.[10,11] Due to the long lifetime (milliseconds) of lanthanides, the large Stokes shift, and Förster radii up to 9 nm, LRET efficiencies can be determined over a wide range of distances (1−14 nm). However, a wider applicability to cell measurements has to date been limited due to the lack of suitable bright and photostable lanthanide complexes and difficulties to specifically attach these probes to proteins or subcellular structures.[12] In addition, LRET measurements require a modulated, high-intensity UV excitation source and a time-gated detection rarely offered by standard microscopes.

In this study, we present an approach for FRET efficiency estimation that exploits the triplet state of the A fluorophore. The triplet state population of any fluorophore is sensitive to its excitation rate, independent of whether the fluorophore is excited directly or via FRET. For low FRET efficiencies, also small absolute changes in E, and thus also of changes in the excitation rate of A,

Received: July 15, 2011
Revised: September 16, 2011
Published: September 19, 2011

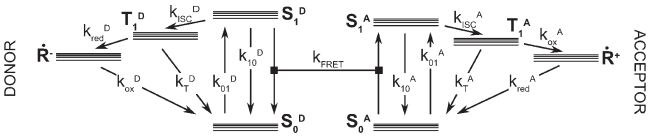

Figure 1. Electronic state model of D and A coupled via FRET with rate constant k_{FRET}. Each molecule consists of a ground and an excited singlet state, S_0 and S_1, the first excited triplet state, T_1, and a radical state $\dot{R}^+/\dot{R}^-$. k_{01}, k_{10}, k_{ISC}, k_T, k_{ox}, and k_{red} denote the rate constants for excitation and de-excitation of the singlet state, intersystem crossing and de-excitation of the triplet state, and oxidation and reduction rate of the radical state, respectively. Upper indices D,A relate the corresponding rates or states to the donor or acceptor molecule.

can strongly influence the population of the A-triplet state due to its relatively long lifetime (microseconds). This makes it possible to distinguish between low FRET efficiencies generated from D−A distances of more than 10 nm, also when standard organic fluorophores are used. The approach is demonstrated by determining FRET efficiencies of DNA samples labeled with the fluorophores ATTO 488 and Alexa Fluor 610. First, we present the basic principle of the method by using fluorescence correlation spectroscopy (FCS) to monitor the A-triplet state. In a second step, we look into the possibility of applying FRET triplet state measurements to a broader range of microscopic techniques. This is done by adapting the recently developed transient state (TRAST) monitoring technique to the FRET triplet state measurements.[13−15] In TRAST, the A-triplet state is deduced by modulating the excitation of D in a well-defined on−off fashion and detecting the A fluorescence for different pulse settings. The same kind of on−off modulation can be obtained by scanning a laser beam over the image region with different scanning speeds.[16] This indicates that our approach can determine the A-triplet state, and hence FRET efficiencies, in a wide range of microscopy settings, including confocal laser scanning microscopy and fluorescence-based plate readers. The determined FRET efficiencies are compared with theoretical values obtained from a standard DNA model[17] and with fluorescence lifetime measurements of the donor.

Due to a novel suppression algorithm for D bleed-through, substantial fractions of incompletely labeled FRET molecules can be tolerated, and D−A pairs with large Förster radii can be used with only minor concerns regarding the spectral overlap of D and A. Taken together, A-triplet state measurements are able to distinguish FRET efficiencies even below 5%, and D−A distances well beyond the 10 nm limit of conventional FRET methods can be detected.

THEORY

Electronic State Model. To compute the FRET efficiencies, we use an electronic state model consisting of a D and an A fluorophore coupled by energy transfer with a rate k_{FRET} (Figure 1). Each individual molecule comprises a ground and an excited singlet state (S_0 and S_1), the lowest triplet state (T_1), and a photooxidized ($\dot{R}^+$) or -reduced ($\dot{R}^-$) radical state. Transitions between S_0 and S_1 are quantified by the fluorescence decay rate $k_{10} = 1/\tau_F$ (τ_F is the fluorescence lifetime) and by the excitation rate $k_{01}(\vec{r},t) = \sigma_{exc} I_{exc}(\vec{r},t)$. Here, σ_{exc} is the excitation cross section for transitions from S_0 to S_1, and $I_{exc}(\vec{r},t)$ is the excitation intensity at a location $\vec{r}$ within the laser beam. k_{ISC}, k_T, k_{ox}, and k_{red} denote the intersystem crossing rate, the triplet relaxation rate, the oxidation rate, and the reduction rate, respectively. Oxidation is usually assumed to originate from S_1 and T_1. However, since the populations of S_1 and T_1 only differ by a scaling factor and k_{ox} and k_{red} are well separated in time from the triplet transitions, oxidation is for simplicity assumed to occur only from T_1.[18] For an individual fluorophore, the probability of being in a certain state (S_0, S_1, T_1, or $\dot{R}^+$) at a location $\vec{r}$ and time t can be calculated by a system of four first-order differential equations.

$$\frac{d}{dt}\begin{pmatrix} S_0(\vec{r},t) \\ S_1(\vec{r},t) \\ T_1(\vec{r},t) \\ \dot{R}^+(\vec{r},t) \end{pmatrix} = \begin{bmatrix} -k_{01}(\vec{r},t) & k_{10} & k_T & k_{red} \\ k_{01}(\vec{r},t) & -(k_{10}+k_{ISC}) & 0 & 0 \\ 0 & k_{ISC} & -(k_T+k_{ox}) & 0 \\ 0 & 0 & k_{ox} & -k_{red} \end{bmatrix} \begin{pmatrix} S_0(\vec{r},t) \\ S_1(\vec{r},t) \\ T_1(\vec{r},t) \\ \dot{R}^+(\vec{r},t) \end{pmatrix} \quad (1)$$

For a fluorophore with a photoreduced radical state $\dot{R}^-$, eq 1 can be modified by exchanging $\dot{R}^+$ with $\dot{R}^-$ and interchanging k_{ox} and k_{red}. Equation 1 can also be applied to the D or A of a FRET pair with energy transfer occurring from S_1^D to S_0^A as well as to T_1^A, but not to the radical state of A.[19] For the donor, the fluorescence decay rate is substituted with

$$k_{10}^{D,tot} \equiv k_{10}^D + k_{FRET}(S_0^A(\vec{r},t) + T_1^A(\vec{r},t)) \approx k_{10}^D + k_{FRET} \quad (2)$$

while the excitation rate of A is replaced by

$$k_{01}^{A,tot}(\vec{r},t) \equiv k_{01}^A(\vec{r},t) + k_{FRET} S_1^D(\vec{r},t), \text{ with}$$
$$S_1^D(\vec{r},t) = \frac{k_{01}^D(\vec{r},t) k_T^D}{k_{01}^D(\vec{r},t)(k_{ISC}^D + k_T^D) + k_{10}^{D,tot} k_T^D} \quad (3)$$

(Figure 1). In eqs 2 and 3 and from now on, upper case, superscript letters D,A indicate whether a rate or a state belongs to the donor or acceptor, respectively. Under our experimental conditions, $\dot{R}^{+A}$ can be neglected in the A-triplet state analysis in FCS (the typical transit time of the studied molecules through the laser excitation beam was 300 μs, and the time range of the $\dot{R}^{+A}$ state build-up was in the range of milliseconds; eq 1 can then be approximated as a three-state model of S_0, S_1, and T_1) and in TRAST (Following the onset of excitation, the relaxation time for the A-triplet state build-up was 3 μs. The corresponding relaxation time for the $\dot{R}^{+A}$ state build-up was in the millisecond time scale, i.e., well after the equilibration of the triplet state). Given that S_1^A is typically <0.05, the boundary condition of eq 1 ($S_0^A + S_1^A + T_1^A + \dot{R}^{+A} = 1$) can be simplified to $S_0^A + T_1^A \approx 1$. Excitation of S_1^A and T_1^A into higher excited singlet and triplet states, S_n^A and T_n^A, is excluded from the electronic state model of eq 1 because S_n^A and T_n^A are only sparsely populated due to the moderate excitation irradiances used (<120 kW/cm^2)[18,20,21] and the short lifetimes of those states (femtoseconds).[20]

FRET efficiencies E can be calculated from the FRET rate by

$$E = \left(\frac{k_{10}^D}{k_{FRET}} + 1\right)^{-1} \quad (4)$$

Triplet State Kinetics from FCS. In FCS, fluorescence fluctuations from individual molecules are studied as they diffuse

in and out of an observation volume defined by the focus of a laser beam. The detected fluorescence $\overline{F}(t)$ depends on the detection quantum yield of the instrument (Φ_{det}), the fluorescence quantum yield of the fluorophore (Φ_F), the collection efficiency function CEF($\vec{r}$), and the fluorophore concentration $c(\vec{r},t)$.

$$\overline{F}(t) = \int F(\vec{r},t)\mathrm{d}V = \int \Phi_{det}\Phi_F \mathrm{CEF}(\vec{r})\sigma_{exc}I_{exc}(\vec{r},t)c(\vec{r},t)\mathrm{d}V \quad (5)$$

The intrinsic fluorescence fluctuations, δF, of $\overline{F}(t)$ under a constant excitation intensity ($I_{exc}(\vec{r},t) := I_{exc}(\vec{r})$) can be described by the autocorrelation function $G(\tau)$.

$$G(\tau) = \frac{\langle F(t)F(t+\tau)\rangle}{\langle F(t)\rangle^2} - 1 = \frac{\langle \delta F(t)\delta F(t+\tau)\rangle}{\langle F(t)\rangle^2} = \frac{1}{N(1-\sum_{x=1,\ldots,n}\overline{T}^x)}\left(\frac{1}{1+\tau/\tau_D}\right) \times \left(\frac{1}{1+(\omega_0/\omega_z)^2\tau/\tau_D}\right)^{1/2} \cdot \prod_{x=1,\ldots,n} G_T^x(\tau)$$
$$G_T^x(\tau) \equiv 1 - \overline{T}^x + \overline{T}^x \exp(-\tau/\overline{\tau}_T^x) \quad (6)$$

Here, $G(\tau)$ is shown for one diffusing species and n different independent dark states $G_T^x(\tau)$. The angle brackets indicate time averages; $\tau_D = \omega_0^2/4D$ is the diffusion time of the studied molecules with a diffusion coefficient D; N is the average number of molecules in the detection volume; and ω_0 and ω_z denote the distance from the center of the detection volume in the radial and axial direction, respectively, at which $F(t)$ is decreased by a factor of $1/e^2$. $G_T^x(\tau)$ contains information about the average population of molecules in the detection volume that are in the dark state, $\overline{T}^x$, and their average relaxation time $\overline{\tau}_T^x$.

In the FCS analysis, A and D are described by a three-state model of S_0, S_1, and T_1, and the resulting triplet state rates k_{ISC} and k_T can be derived from the average triplet state population $\overline{T}$ and the corresponding relaxation time $\overline{\tau}_T$ as described in ref 22.

The A-triplet state is dependent on the A excitation rate, which in turn is proportional to the FRET efficiency. Therefore, the A-triplet state parameters, $\overline{T}^A$ and $\overline{\tau}_T^A$, determined from A correlation curves, are related not only to the triplet state rates k_{ISC}^A and k_T^A but also to the FRET rate k_{FRET} in analogy to the FRET-modified electronic state model in eq 1.

$$T^A(\vec{r}) = \frac{k_{01}^{A,tot}(\vec{r})k_{ISC}^A}{k_{01}^{A,tot}(\vec{r})(k_{ISC}^A + k_T^A) + k_{10}^A k_T^A}$$
$$\tau_T^A(\vec{r}) = \left[k_T^A + \frac{k_{01}^{A,tot}(\vec{r})k_{ISC}^A}{k_{01}^{A,tot}(\vec{r}) + k_{10}^A}\right]^{-1} \quad (7)$$

Here, $T^A(\vec{r})$ and $\tau_T^A(\vec{r})$ are defined at any location $\vec{r}$ in the excitation volume. Subsequent integration of $T^A(\vec{r})$ and $\tau_T^A(\vec{r})$ over the whole detection volume, weighted with $<F(t)>^2$, yields $\overline{T}^A$ and $\overline{\tau}_T^A$, respectively.[22] By knowing k_{ISC}, k_T, k_{10}, and σ_{exc} of A and D beforehand, one can solve eqs 3, 4, and 7 to yield k_{FRET} and the corresponding FRET efficiency.

Triplet State and Redox Kinetics from TRAST. Transient state monitoring (TRAST) has been applied previously to determine triplet and radical state properties of fluorophores.[14−16] In TRAST, the excitation intensity is modulated in an on−off fashion while recording the time-averaged fluorescence response. During each excitation pulse, the triplet and radical state populations build up over time, leading to a decrease in fluorescence. By investigating the change in average fluorescence for different pulse widths and/or pulse periods, the populations of nonfluorescent states can be monitored.

TRAST is applied as described by Spielmann et al.[15] but in a confocal instead of a total-internal-reflection microscope setting. The Gaussian−Lorentzian excitation profile is approximated by a rectangular homogeneous excitation profile yielding the same overall exciation power: $k_{01}(\vec{r},t) \equiv \overline{k}_{01}(t)$. Thus, $\overline{k}_{01}$ is the averaged excitation rate contributing to the fluorescence $\overline{F}(t)$, where $\overline{F}(t)$ is integrated over the focal spot as described in eq 5. This approximation has been used previously for FCS measurements[20,23] and allows extracting reasonable estimates of triplet parameters from TRAST measurements while simplifying the analysis substantially.

The time-resolved fluorescence response, $\overline{F}(t)$, during a given excitation pulse can then be calculated by solving the rate equations of eq 1 for the excited singlet state population, $\overline{S}_1(t)$. The duty cycle, which is the ratio of the pulse width to the pulse period, was kept low to limit bleaching and depletion effects.[15] A low duty cycle also ensures that the system has completely relaxed at the onset of every new pulse in the pulse train (i.e., all molecules then reside in S_0). As the singlet, triplet, and redox kinetics are well separated in time (nanoseconds, microseconds, and milliseconds), they can be treated independently. Moreover, the singlet state kinetics are generally too fast to be resolved by the present instrumentation. Therefore, for any individual fluorophore, the average fluorescence emitted during a pulse of width w can be approximated by

$$\overline{F}(w) = \overline{F}_0\left\{\frac{\overline{k}'_{ISC}}{-(\overline{k}'_{ISC}+k_T)^2 w}(e^{-(\overline{k}'_{ISC}+k_T)w}-1) + \frac{k_T}{\overline{k}'_{ISC}+k_T} \times \left[\frac{\overline{k}'_{ox}}{-(\overline{k}'_{ox}+k_{red})^2 w}(e^{-(\overline{k}'_{ox}+k_{red})w}-1) + \frac{k_{red}}{\overline{k}'_{ox}+k_{red}}\right]\right\} \quad (8)$$

In eq 8, $\overline{k}'_{ISC}$ denotes the equivalent intersystem crossing from the two singlet states (S_0 and S_1) to the triplet state T_1, and $\overline{k}'_{ox}$ is the equivalent oxidation rate (from $S_0 + S_1 + T_1$) to the radical state $\dot{R}^+$

$$\overline{k}'_{ISC} = k_{ISC}\frac{\overline{k}_{01}}{\overline{k}_{01}+k_{10}} \qquad \overline{k}'_{ox} = k_{ox}\frac{\overline{k}'_{ISC}}{\overline{k}'_{ISC}+k_T} \quad (9)$$

Moreover, in eq 8, $\overline{F}_0$ represents the average fluorescence count rate in the absence of transient populations of T_1 and $\dot{R}^+$ and is proportional to the detection efficiency Φ_D, the fluorophore concentration $\bar{c}$, the excitation volume V_{exc}, and the fluorescence quantum yield Φ_F.

$$\overline{F}_0 = \Phi_D \bar{c} V_{exc}\Phi_F \frac{k_{10}\overline{k}_{01}}{k_{10}+\overline{k}_{01}} \quad (10)$$

Here, we are only interested in relative changes in $\overline{F}(w)$ that originate from the build-up of transient states (e.g., T_1 and $\dot{R}^+$). Therefore, $\overline{F}(w)$ is normalized to unity for w shorter than the triplet relaxation time.

To determine FRET efficiencies, $\overline{k}_{01}$ in eqs 9 and 10 is substituted by $\overline{k}_{01}^{A,tot}(\vec{r},t)$ in analogy to eq 3. Furthermore, the expression for $\overline{S}_1^D$ can be simplified in the analysis because the build-up of the D triplet state can be neglected in the presence of millimolar concentrations of potassium iodide[24] and for the moderate excitation rates used in the TRAST measurements ($k_{ISC}^D < k_T^D$).

MATERIALS AND METHODS

FCS. Measurements were performed on an epi-illuminated confocal microscope (Leitz).[25] The light of an argon-ion laser (488 nm; Lasos, Jena, Germany) or an argon−krypton ion laser (488 nm, 568 nm; Melles Griot, Carlsbad, CA, USA) was filtered (488/10 nm, 568/10 nm, Chroma Technology Corp., Rockingham, VT, USA), focused in front of the microscope, reflected by a dichroic mirror (Z488RDC, Chroma Technology Corp.; FF576/661, Semrock, Rochester, NY, USA), and focused on the image plane by a water-immersion objective (63x/1.2 Plan-Neofluar, 160 mm tube length; Zeiss, Oberkochen, Germany). The intensity distribution is assumed to be Gaussian distributed in the radial direction and Lorentzian distributed in the axial direction, with a focal diameter of ~0.7 μm. The resulting fluorescence was collected by the same objective, focused onto a 50 μm pinhole, band-pass filtered (532/70 nm, filter 1: 675/135 nm, blue-shifted filter 2: 640/115 nm; Chroma Technology Corp.), split by a 50/50 beam splitter (Thorlabs, Newton, NJ, USA), and focused onto two single-photon-counting avalanche photodiodes (SPCM-AQR-14, PerkinElmer Optoelectronics, Waltham, LA, USA). The signals of the two detectors were processed by a correlator (ALV-5000, ALV GmbH, Langen, Germany) and then further analyzed using custom software. The oxygen concentration in the buffer solution was strongly reduced by applying a flow of argon over the sample droplet.

TRAST Measurements. The instrumentation was based on a previously described setup for total internal reflection fluorescence microscopy, used here in a confocal setting.[15] Briefly, a solid state laser (Calypso, Cobolt AB, Solna, Sweden; 491 nm) was focused onto an acousto-optic modulator (AOM, MQ 180−AO, 25-VIS, AA Opto-Electronic, Orsay, France) to yield the on−off modulation. After the AOM, the laser beam was collimated and reflected by a dichroic mirror (F500-Di01, Semrock Inc.) onto the objective (40x/1.2 C-Apochromat, water immersion, Zeiss). The resulting radial focus spot diameter was estimated to ~2 μm. The emitted fluorescence was collected with the same objective, band-pass filtered (675/135 nm, 530/50 nm, Chroma Technology Corp.), and focused onto an electron multiplying CCD (Luca, Andor Technology, Belfast, Northern Ireland, United Kingdom; used in quarter screen mode, 330 × 248 pixels). The modulation scheme of the AOM was set by a National Instruments (Austin, TX, USA) PCI 6602 card connected to the modulator controller (AA Opto Electronic). The camera, diode laser, and National Instruments card were controlled via custom Matlab software.

Reference TRAST measurements on Rhodamine 110 (Rh110) were performed to relate the used laser intensities to the $\overline{k}_{01}^D$ rate in eqs 9 and 10. For the excitation intensities used in this study, the Rh110 excitation rate $\overline{k}_{01}^{Rh110}$ was calculated by fitting measurements to eqs 8 and 9 with fixed photophysical parameters ($k_{ISC}^{Rh110} = 10^6\ s^{-1}$, $k_T^{Rh110} = 0.45 \times 10^6\ s^{-1}$, $k_{10}^{Rh110} = 244 \times 10^6\ s^{-1}$ [26]). The D-excitation rate was then calculated according to $\overline{k}_{01}^D := (\sigma_{exc,491}^D)/(\sigma_{exc,491}^{Rh110})\overline{k}_{01}^{Rh110}$, with $\sigma_{exc,491}^{Rh110} = 2.9 \times 10^{-16}\ cm^2$ and $\sigma_{exc,491}^D = 2.5 \times 10^{-16}\ cm^2$. The direct excitation $\overline{k}_{01}^A$ of A by laser light was estimated using $\sigma_{exc,491}^A = 0.08 \times 10^{-16}\ cm^2$. $\sigma_{exc,491}^{D,A}$ and $\sigma_{exc,491}^{Rh110}$ were obtained by using literature values of the maximum extinction coefficient (as specified by Invitrogen Inc. and ATTO-TEC GmbH) and then calculating the extinction coefficient of a certain wavelength in relation to the measured fluorescence spectra. Extinction coefficients for FCS were determined in a similar fashion to $\sigma_{exc,488}^D = 2.243 \times 10^{-16}\ cm^2$ and $\sigma_{exc,488}^A = 0.079 \times 10^{-16}\ cm^2$.

Fluorescence Lifetime and Spectrum Measurements. Measurements were performed on a spectrofluorometer capable of time-correlated single-photon counting (FluoroMax-3, Horiba, Longjumeau, France; excitation source for lifetime measurements: NanoLED 495 nm). Lifetime decay data were analyzed by least-squares deconvolution of a one-component exponential decay for D-only samples ($\tau_{F,D}$) and deconvolution of a 2−3 exponential decay model for D−A samples (DAS6, Horiba) with lifetimes τ_i and amplitude A_i, with $\sum_i A_i = 1$. For the donor fluorophore in the presence of an acceptor, an average lifetime

$$\tau_{F,DA} = \tau_1 A_1 + \tau_2 A_2 + \tau_3 A_3 \quad (11)$$

was calculated and used for further FRET efficiency calculations

$$E = 1 - \tau_{F,D}/\tau_{F,DA} \quad (12)$$

The fluorescence decay rate in the absence of FRET was calculated from the fluorescence lifetime of A-only or D-only labeled samples by $k_{10}^{D,A} = \tau_F^{-1}$.

Sample Preparation. As a model system, we used highly purified double-stranded DNA (Purimex, Grebenstein, Germany) with ATTO 488 (ATTO-TEC GmbH, Siegen, Germany) and Alexa Fluor 610 (Invitrogen Inc., Eugene, OR, USA) labeled onto different positions of the DNA strand. The DNA lead strand CCT TTC AGG AGG GAA GAG AGA GAG GAA AAT CAA ATC CTC CTA AGG G was either unmodified (control measurements) or modified at position three with ATTO 488 attached via a C_6 linker. The complementary strand CCC TTA GGA GGA TTT GAT TTT CCT CTC TCT CTT CCC TCC TGA AAG G was unmodified or modified with Alexa Fluor 610 attached via a C_6 linker at position 13, 18, 23, 27, 29, 32, or 44. Hybridization of double-stranded DNA (dsDNA) was performed by adding lead and complementary strands in a concentration ratio of 2:1 (FCS) or 1:3 (lifetime measurements) to a Tris buffer (20 mM Tris, 50 mM NaCl, 10 mM $MgCl_2$, pH 7.5). The DNA strands were incubated at 95 °C for 5 min and gradually cooled to room temperature over 3 h. dsDNA was diluted to nanomolar concentration in Tris buffer with or without potassium iodide (KI; Sigma-Aldrich, St. Louis, MO, USA). If not stated otherwise, samples were measured in air-saturated Tris buffer with 5 mM KI.

DNA Model. FRET efficiencies were estimated from a standard DNA model with D and A fluorophore attached to a double-stranded helix of B-DNA.[17] The helix had a width of 2 nm, a helical turn, $\Delta\alpha$, of 36 degrees per base pair, and a distance d_{bp} = 0.338 nm between two consecutive base pairs. The dyes were linked to the DNA by a carbon linker consisting of six carbon atoms (estimated length: C_6 = 0.6 nm) protruding perpendicular from the DNA body. The average distance d_{DA} between the donor and acceptor with Δbp base pairs between them was calculated according to

$$d_{DA} = [2(1 + C_6)^2(1 - \cos(\Delta bp \Delta\alpha)) + \Delta bp^2 d_{bp}^2]^{1/2} \quad (13)$$

Subsequently, the corresponding FRET efficiency

$$E = [1 + (d_{DA}/R_0)^6]^{-1} \quad (14)$$

was computed. Here, R_0 denotes the Förster radius of the FRET pair.

$$R_0 = [8.79 \times 10^{-4} J(\lambda)\Phi_F^D n^{-4}\kappa^2]^{1/6} \quad (15)$$

R_0 depends on the spectral overlap integral $J(\lambda)$ between the fluorescence spectrum of D and the absorption spectrum of A; Φ_F of D in the absence of A; the refractive index n of the medium; and the orientation factor of D and A dipole moments, κ^2. For ATTO 488 and Alexa 610, the Förster radius was computed to 5.6 nm ($\Phi_F^D = 0.7$, assumed random orientation of D−A dipole moments: $\kappa^2 = 2/3$, $n = 1.337$, $J(\lambda) = 2.344 \times 10^{-13}$ cm^3 M^{-1}).

RESULTS

1. Effects of Potassium Iodide on the FRET Pair. The triplet state population of a fluorophore strongly depends on the excitation rate, no matter how the fluorophore is excited (eq 7). Hence, when an acceptor is excited by FRET, its triplet state population can be used as a measure of the FRET efficiency and the corresponding D−A distance. To ensure a substantial triplet state build-up of A, relatively high I_{exc} values are required. This may lead to a considerable triplet state build-up of D. When D is in its triplet state, no FRET will occur between D and A. The singlet−triplet state transitions of D thereby superimpose a modulation on the A-excitation and on its fluorescence. The resulting A-fluorescence fluctuations are then difficult to separate from those resulting from A-triplet state transitions. These complications can be circumvented by addition of potassium iodide (KI) to the solvent.

In millimolar concentrations, KI is known to promote intersystem crossing to the triplet state due to a heavy atom effect in all dyes.[24] For many dyes with an excitation maximum in the blue range, it additionally enhances the triplet state decay rate by a charge-transfer-mediated interaction between the fluorophore and iodide. Taken together, addition of KI in millimolar concentrations can result in a reduced triplet state build-up for dyes in the blue excitation range and an increased triplet state build-up for dyes with excitation maxima in the green range or longer. In this study, we exploited the effect of KI to markedly reduce the triplet state build-up of D and minimize fluctuations in the A excitation. The KI-mediated increase in the triplet state build-up of A makes it more sensitive to changes in excitation intensity and hence to differences in FRET efficiency.

The triplet state kinetics of the two dyes responded to potassium iodide (KI) as reported in ref 24, including also a KI-induced build-up of a photoreduced radical state $\dot{R}^{-D}$ of ATTO 488 in proportion to the applied KI concentration. A concentration of 5 mM KI was identified as the best compromise between maintaining a low amount of $\dot{R}^{-D}$ formation while decreasing the ATTO 488 triplet state population and increasing the Alexa 610 triplet state population (Figure 2). When KI was added, the measured triplet fraction of ATTO 488 bound to DNA was reduced from maximally 40% in the absence to maximally 10% in the presence of KI. The corresponding triplet relaxation time shifted from several microseconds to 0.2 μs for all I_{exc} applied. The largest $\dot{R}^{-D}$ population was 10% with relaxation times of 10 μs. In contrast, the maximum triplet fraction of Alexa 610 bound to dsDNA increased from 50% to 60% after addition of KI, while the triplet relaxation time remained constant (2−3 μs). The relaxation times of the triplet states of ATTO 488 and Alexa 610 as well as of the ATTO 488 radical state were each separated by an order of magnitude and could therefore be clearly distinguished and separated in the analysis.

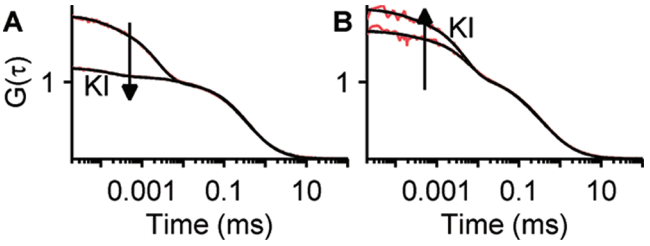

Figure 2. Influence of potassium iodide (KI) on D and A bound to dsDNA. Experimental (red line) and fitted (black line) correlation curves are shown for D and A in the absence and presence of KI. (A) In the presence of 5 mM KI, the triplet state population of ATTO 488 is decreased (indicated by the arrow) and shifted to faster times (2.5 μs → 0.2 μs). $I_{exc,\ 488\ nm}$, 189 kW/cm^2; emission filter, 532/70 nm. (B) The triplet fraction of Alexa 610 increases upon addition of KI (indicated by the arrow), while the triplet relaxation time remains constant at 3 μs. $I_{exc,568\ nm}$, 28 kW/cm^2; emission filter, 640/115 nm.

$k_{ISC}^{D,A}$, $k_T^{D,A}$, k_{red}^D, and k_{ox}^D were obtained by direct excitation of ATTO 488-only or ATTO488-Alexa 610 labeled dsDNA (excitation: 488 or 568 nm). The correlation curves for ten I_{exc} (6−500 kW/cm^2) were each analyzed by eq 6 using one diffusion component and one (acceptor; T_1) or two (donor; T_1, $\dot{R}^{-D}$) dark states. The resulting $\overline{T}$ and $\overline{\tau}_T$ for all I_{exc} were simultaneously fitted to eq 7 according to the electronic state model of a single fluorophore (eq 1). In these global fits, $k_{ISC}^{D,A}$ and $k_T^{D,A}$ were free to vary, while $\sigma_{exc,488}^{\ D} = 2.243 \times 10^{-16}$ cm^2, $\sigma_{exc,568}^{A} = 1.667 \times 10^{-16}$ cm^2, $k_{10}^D = 265 \times 10^6$ s^{-1}, and $k_{10}^A = 255 \times 10^6$ s^{-1} were kept constant. At 5 mM KI, the triplet rates were found to be $k_{ISC}^D = 2.0 \times 10^6$ s^{-1}, $k_T^D = 5.1 \times 10^6$ s^{-1}, $k_{ISC}^A = 1.4 \times 10^6$ s^{-1}, and $k_T^A = 0.13 \times 10^6$ s^{-1}. k_{red}^D and k_{ox}^D were determined from the redox state amplitude and relaxation time in analogy to refs 18 and 24 to $k_{red}^D = 0.025 \pm 0.003 \times 10^6$ s^{-1} and $k_{ox}^D = 0.1 \pm 0.01 \times 10^6$ s^{-1}.

2. FRET Efficiencies Determined by FCS. *Acceptor FCS Curves Show a FRET-Dependent Triplet State Population.* By addition of KI, the D-triplet state was sufficiently suppressed, and hence an almost continuous FRET-mediated excitation of A could be ensured. In the measurements, D was directly excited, and A-autocorrelation curves were recorded for different I_{exc} (6−120 kW/cm^2) and D−A distances (10−41 Δbp). In addition to the diffusion of the molecules, three dark state relaxation processes were identified in the autocorrelation curves: the D-triplet ($\overline{\tau}_T^D \approx 0.2$ μs), the A-triplet ($\overline{\tau}_T^A \approx 3$ μs), and the D-radical state ($\overline{\tau}_R^D \approx 15$ μs). Examples of the resulting A-autocorrelation curves are shown in Figure 3. As expected, the triplet state population increased, and the triplet state relaxation time decreased with shorter D−A distances. However, for certain D−A distances, differences observed in the autocorrelation curves were smaller than expected. For instance, the correlation curves from samples 41 Δbp and 26 Δbp as well as 10 Δbp and 15 Δbp are relatively closely spaced in Figure 3. A possible reason can be large subfractions of D-only or A-only labeled species that will bias the detected average triplet state population to lower values. The influence of incompletely labeled FRET pairs is a problem for most FRET measurements and usually requires extended control measurements to compensate for. In the following chapter, we will propose a procedure that will correct for D-only labeled samples without the need for complicated control measurements or additional samples.

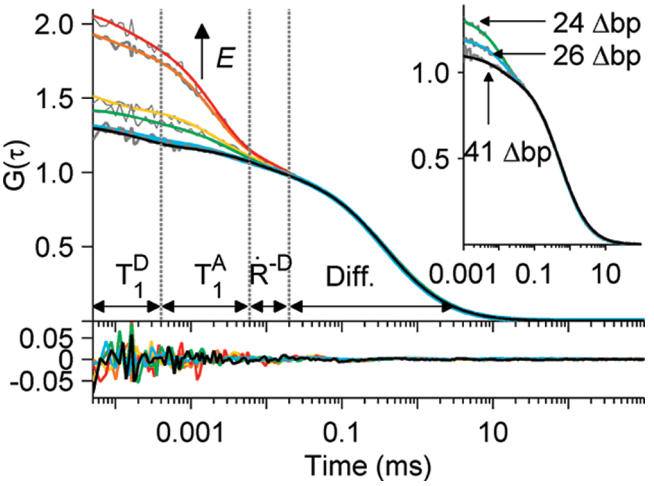

Figure 3. A-correlation curves for FRET-mediated excitation of oligonucleotides with different D−A base pair separations Δbp. The experimental (gray line) and fitted (Δbp = 10, red line; 15, orange line; 20, yellow line; 24, green line; 26, blue line; 41, black line) correlation curves (eq 6) consist of one diffusion component (Diff., $\tau_D \sim 350\,\mu s$) and three dark states corresponding to the D-triplet (T_1^D, $\overline{\tau}_T^D \sim 0.2\,\mu s$), the A-triplet ($T_1^A$, $\overline{\tau}_T{}^A \sim 3\,\mu s$), and the D-radical state ($\dot{R}^{-D}$, $\overline{\tau}_R{}^D \sim 10\,\mu s$). Corresponding residuals are shown below. The A-triplet state population increases in proportion to the FRET efficiency *E*. $I_{exc,488\ nm}$, 119 kW/cm^2; emission filter, 675/135 nm. Inset: A-correlation curves for different FRET samples in a low oxygen solution under argon flow. Applying an argon flow markedly increases the triplet state population and the difference in the triplet state populations especially for low-FRET samples.

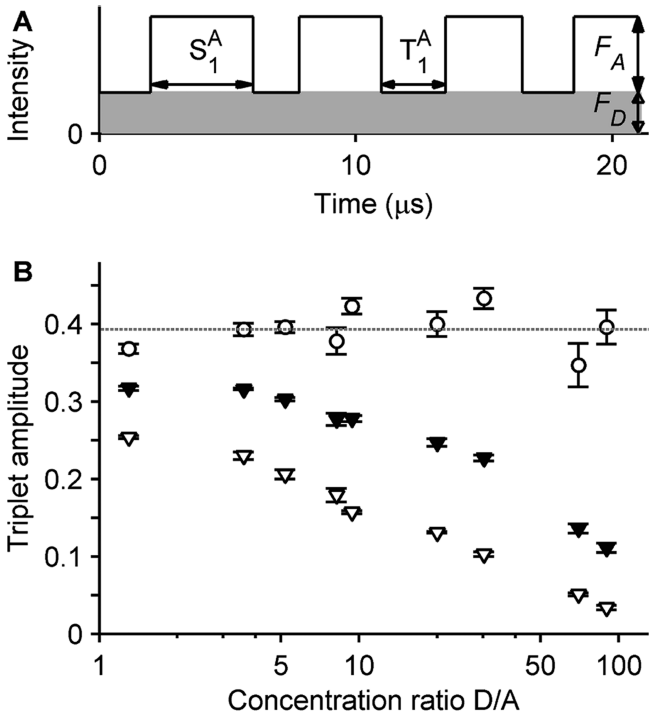

Figure 4. Influence of D-only labeled samples on the A-triplet amplitude. (A) Fluorescence signal detected in the A channel. The signal consists of A fluorescence, F_A, and D fluorescence, F_D, leaking into the channel. The modulation in the signal originates mainly from singlet−triplet transitions ($S_1{}^A$−$T_1{}^A$) of A. The singlet−triplet transitions of D are suppressed by KI, thereby ensuring an almost constant excitation of A via FRET. (B) Correction of $\overline{T}^A$, which was determined from A-autocorrelation curves for FRET-mediated excitation. Because of spectral bleed-through, the measured average triplet state population from a DA-labeled dsDNA sample with Δbp = 15 (▼, filter 1) decreased upon addition of D-only-labeled dsDNA. Applying a slightly blue-shifted emission filter 2 decreased the measured triplet state population (▽) even further. The influence of the spectral bleed-through could be eliminated by applying the correction procedure described in the text. The resulting real $\overline{T}^A$ (○) could be recovered over the full range of D/A concentrations. The dashed line represents the mean value of all recovered $\overline{T}^A$. Data points represent the mean value of six measurements and the corresponding standard deviation in those. $I_{exc,488\ nm}$, 55 kW/cm^2; emission filter 1, 675/135 nm, d_1 = 3.45%, a_1 = 79.7%; emission filter 2, 640/115 nm, d_2 = 9.01%, a_2 = 80.4%.

Apart from addition of KI, oxygen can be removed from the buffer solution to increase the FRET sensitivity of A-triplet state measurements (Figure 3, inset). Oxygen is known to promote the triplet state transitions, in particular the relaxation from T_1 to S_0. Hence, removal of oxygen from the buffer typically leads to an increase in the triplet state population of the dye. When applying 5 mM KI and diminishing the oxygen concentration in the buffer, the effect of KI on the dyes predominated: $k_{ISC}^{D,A}$ and k_T^D did not drastically change while k_T^A was reduced to $k_T^A = 0.06 \times 10^6\ s^{-1}$. Hence, the D-triplet state population was found to remain low, while the A-triplet state population was found to clearly increase upon low oxygen concentrations. From eq 7, it follows that differences in low excitation rates then lead to larger absolute differences in $\overline{T}^A$. In line with this, we noted that upon reduction of oxygen concentration and addition of KI, samples with low FRET efficiencies could be far better distinguished from each other (~150% increase in the difference of the A-triplet fraction between the 41 Δbp and 26 Δbp sample). A complete removal of oxygen, however, may also lead to a stronger build-up of $\dot{R}^{-D}$ since oxygen can quench this state.[18] Therefore, oxygen was not fully removed in these measurements.

Donor Bleed-through Correction. To enhance the resolution and minimize the influence of D-only labeled specimen on the FRET efficiency, a procedure was introduced to correct for the spectral bleed-through of D fluorescence.

The detected emission signal consists of A fluorescence and D fluorescence leaking into the detection channel (Figure 4A). Both, D and A fluorescence contribute to the diffusion part of the autocorrelation curve. While the D-triplet state population has a negligible amplitude with $\tau_T^D \approx 0.2\,\mu s$, A has a prominent triplet state population with $\tau_T^A \approx 2\,\mu s$. Because the autocorrelation analysis does not differentiate between D and A fluorescence, the detected triplet state in the microsecond range will be an average of the D- and A-triplet state, each weighted with the molecular brightness of the corresponding fluorophore in the detection channel. Hence, due to D bleed-through, the measured A-triplet amplitude $\overline{T}_m^A$ will be reduced compared to the actual average triplet state population $\overline{T}^A$ of the acceptor.[27,28]

$$\overline{T}_m^A = \frac{\overline{T}^A(1-Q)^2}{1 + Q^2\overline{T}^A/(1-\overline{T}^A)} \tag{16}$$

Here, *Q* is defined as the ratio of the detected D fluorescence to the A fluorescence.

$$Q = \frac{d \cdot F_D}{d \cdot F_D + a \cdot F_A} \tag{17}$$

dx.doi.org/10.1021/jp206770s |*J. Phys. Chem. B* 2011, 115, 13360–13370

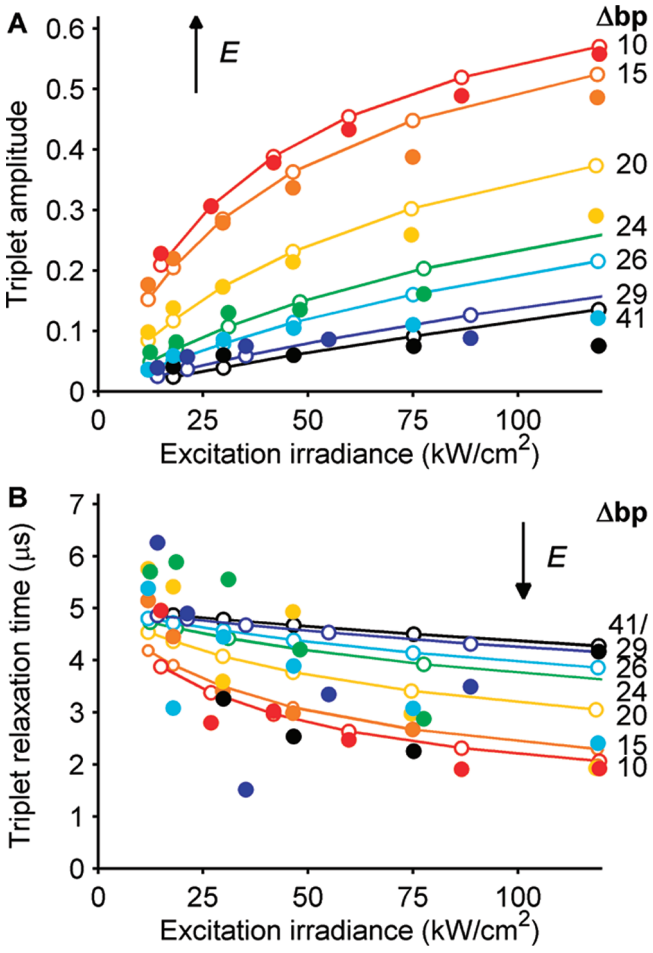

Figure 5. Experimental (filled dots) and fitted (empty dots connected by line) triplet state populations (A) and triplet state relaxation times (B) of A for different FRET oligonucleotides (Δbp = 10, red circle; 15, orange circle; 20, yellow circle; 24, green circle; 26, light blue circle; 29, dark blue circle; 41, black circle). Autocorrelation curves of A were recorded for various $I_{exc,488\ nm}$ (7−120 kW/cm^2) for the emission filters 675/135 nm and 640/115 nm and analyzed (according to eq 6). The real $\overline{T}^A$ were calculated by applying the correction procedure described in the text. $\overline{T}^A$ and $\overline{\tau}_T^A$ were fitted with the electronic state model depicted in Figure 1. Here, k_{ISC}^A and k_T^A were determined from a reference sample with known FRET efficiency (15 Δbp, $E = 0.4$; $k_{ISC}^A = 2.1 \times 10^6\ s^{-1}$, $k_T^A = 0.2 \times 10^6\ s^{-1}$). For a single FRET sample, $\overline{T}^A$ increases in proportion to I_{exc}, whereas $\overline{\tau}_T^A$ decreases with I_{exc}. At a constant I_{exc}, $\overline{T}^A$ increases with increasing E, whereas $\overline{\tau}_T^A$ is reduced at the same time, as indicated by the arrows.

Here, d and a denote the fractions of the D and A fluorescence intensities, F_D and F_A, that are transmitted through the filter. d and a were determined from the emission spectra of D and A and the transmission spectra of the corresponding emission filter and dichroic mirror used in the experiment. The real $\overline{T}^A$ can be calculated by first measuring the A-triplet amplitude $\overline{T}_m{}^A$ of the A fluorophore with an emission filter 1 matched to the spectral region of the A fluorescence ($\rightarrow \overline{T}_{m1}^A$), followed by a second measurement with a slightly blue-shifted A emission filter 2 ($\rightarrow \overline{T}_{m2}^A$). $\overline{T}_{m2}^A$ will be lower than $\overline{T}_{m1}^A$ because of the stronger D bleed-through for filter 2. Using $\overline{T}_{m1}^A$, $\overline{T}_{m2}^A$, and the values determined for $a_{1,2}$ and $d_{1,2}$, $\overline{T}^A$ can be calculated by solving eqs 16 and 17 for the two filters simultaneously.

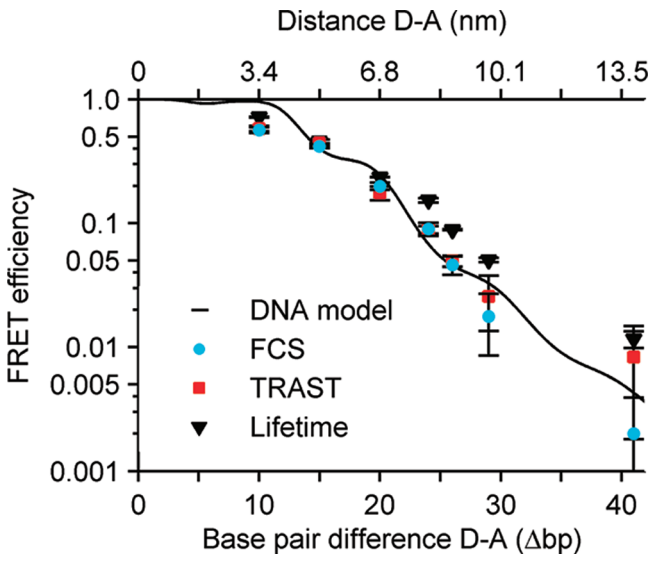

Figure 6. FRET efficiencies obtained for optimal D−A labeling conditions from a theoretical DNA model (−), A FCS (blue ●), A TRAST (red ■), and D lifetime (black ▼) measurements. D−A distances (upper x-axis) were calculated with the dsDNA model according to the D−A base pair difference and a Förster radius of R_0 = 5.6 nm. The corresponding standard errors of the mean of E were determined from 4 (FCS) or 10 (lifetime) measurements. The A-FCS FRET efficiencies agree well with the E calculated from the DNA model, whereas lifetime measurements tend to overestimate E, especially for lower E. The high FRET sample (10 Δbp) is underestimated by both FCS and lifetime measurements due to bleaching (FCS) and a secondary charge transfer process between the D and A through space interactions (FCS, lifetime).

D Bleed-through Correction Compensates for Different A-Labeling Efficiencies. The devised correction of $\overline{T}^A$ is valid not only for D bleed-through of D−A labeled samples but also for incompletely labeled D-only samples as well. The correction procedure was tested on samples of D-only and D−A-labeled dsDNA strands added in different concentration ratios (D-only/D−A = 2−144), and $\overline{T}_{m1}^A$, $\overline{T}_{m2}^A$, and $\overline{T}^A$ were determined for each sample (Figure 4B). With an increasing amount of D-only labeled dsDNA, the measured triplet fraction of A decreased rapidly. Applying the slightly blue-shifted emission filter decreased $\overline{T}_m^A$ even further. However, by applying the bleed-through correction procedure, $\overline{T}^A$ was recovered over the full range of tested D−A ratios. Consequently, by this procedure, A-labeling efficiencies down to 1% could be tolerated while still performing robust FRET measurements.

Acceptor Triplet State Measurements and the FRET Electronic State Model. Being able to correct for donor bleed-through and varying A-labeling efficiencies, we investigated D−A samples for different FRET efficiencies. The donor was excited for seven I_{exc} (7−120 kW/cm^2), and the autocorrelation curve $G(\tau)$ of the A-channel was measured consecutively for the two A-emission filters 1 and 2. $G(\tau)$ was then fitted according to eq 6 including three dark states corresponding to the D-triplet, the A-triplet, and the D-photoreduced state. For each I_{exc}, the measured triplet fractions $\overline{T}_m^A$ of filters 1 and 2 were used to calculate the real $\overline{T}^A$ according to eqs 16 and 17. Subsequently, $\overline{T}^A$ and $\overline{\tau}_T^A$ from all I_{exc} were fitted to eq 7 according to the FRET electronic state model depicted in Figure 1. In this fitting procedure, E was the only free fitting parameter. k_{ISC}^D, k_T^D, k_{ISC}^A, and k_T^A were obtained by FCS measurements by direct excitation of each fluorophore (on dsDNA; see section 1 above) and were kept constant during the

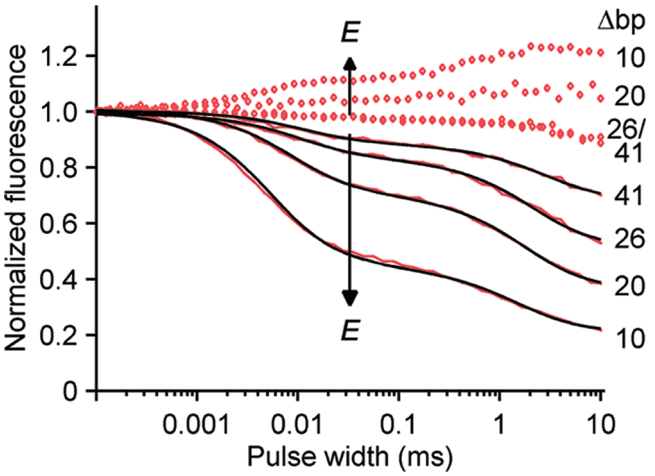

Figure 7. TRAST measurements of different FRET samples with Δbp = 10, 20, 26, and 41 at excitation intensities of I_{exc} = 50 kW/cm^2. The normalized measured (red line) and fitted (black line) A fluorescence decrease with increasing excitation pulse width due to triplet (3 μs) and redox state (2 ms) build-up. The D-fluorescence (red diamond) increases with excitation pulse width due to a reduced energy transfer from D to A because of the triplet and redox state build-up of A. Samples at increasing FRET efficiencies (E) are indicated by the arrows. At similar donor excitation intensities, the decreases in A-fluorescence and the increases in D-fluorescence become more pronounced for higher E. Fitting rates used here: $k^A_{ISC} = 3.6 \times 10^6\ s^{-1}$, $k^A_T = 0.14 \times 10^6\ s^{-1}$, $k^D_{10} = 261.78 \times 10^6\ s^{-1}$, $k^A_{10} = 255.1 \times 10^6\ s^{-1}$.

fitting procedure. As an alternative, or to circumvent the need for a red laser line, k^A_{ISC} and k^A_T can be determined by exciting the D of a FRET sample with known E and detecting the A autocorrelation curve. In this case, the A-triplet state properties $\overline{T}^A$ and $\overline{\tau}^A_T$ can be determined from the A autocorrelation curve and then fitted to eqs 1 and 7 (now with the known E as a constant value) to obtain k^A_{ISC} and k^A_T.

The experimentally determined $\overline{T}^A$ and $\overline{\tau}^A_T$ are in good agreement with the fitted data (Figure 5). For a single FRET sample, $\overline{T}^A$ increases with increasing I_{exc}, while $\overline{\tau}^A_T$ simultaneously decreases. At constant I_{exc}, $\overline{T}^A$ increases with E, while $\overline{\tau}^A_T$ is reduced with increasing E. The different FRET samples can be clearly resolved.

It should be noted that in the presented data analysis E is the only free fitting parameter. This makes the analysis robust, and theoretically, a single data point (sample excited with one I_{exc}) is sufficient to calculate the FRET efficiency. However, to improve the accuracy of E, multiple data points were recorded for each sample at different I_{exc}.

FRET Efficiencies. The FRET efficiencies obtained from the fits of $\overline{T}^A$ and $\overline{\tau}^A_T$ (Figure 5) are shown in Figure 6. The corresponding standard deviations, determined from four measurements, are about 10%.

For comparison, theoretical FRET efficiencies were determined based on the DNA model of a double-helix B-DNA, where the distances between the fluorophores ATTO 488 and Alexa 610 and the corresponding E were calculated based on a Förster radius of 5.6 nm (see Materials and Methods) and according to eqs 13−15. The FRET efficiencies determined with FCS were found to be in adequate agreement with these theoretically calculated FRET efficiencies.

3. FRET Efficiencies Determined by TRAST. Sequentially, the donor was excited with ∼50 different pulse trains whose pulse widths, w, were varied between 100 ns and 10 ms. The pulse height (e.g., the laser intensity) and the pulse train duration were kept constant (I_{exc} between 30 and 80 kW/cm^2 and camera exposure times between 4 and 10 s) at a duty cycle of 1%. For each w, the corrected A fluorescence images were integrated over a circular region (Ø 1.5 μm) in the center of the laser focus. After every fourth pulse train, a calibration measurement was taken at the shortest pulse width to account for concentration changes in the sample.

Donor Bleed-Through Correction. As in the FCS measurements, the detected intensity $\overline{F}$ consisted of D and A fluorescence, $\overline{F} = a \cdot \overline{F}_A + d \cdot \overline{F}_D$. To remove the D bleed-through, the measurement procedure was performed with two emission filters successively: filter 1 matched the A emission spectrum ($\overline{F}_1$), and filter 2 collected only D fluorescence ($\overline{F}_2$; filter 1, 675/135 nm, d_1 = 3.2%, a_1 = 82.7%; filter 2, 530/50 nm, d_2 = 57.6%, a_2 = 0%). By knowing the spectral properties of the dyes, the dichroic mirror, and the two filters, $\overline{F}_A$ was computed for each pulse width according to

$$\overline{F}_A(w) = \frac{1}{a_1}\left(\overline{F}_1(w) - \frac{d_1}{d_2}\overline{F}_2(w)\right)$$

TRAST Confirms FRET-Dependent Triplet State Build-Up. The integrated A fluorescence ($\overline{F}_A$) is plotted against the pulse width (w) for various D−A distances measured at the same I_{exc} (Figure 7). A fast and a slow decrease of $\overline{F}_A$ can be seen for increasing w. These two decreases correspond to two photoinduced processes: the fast process ($w \sim \mu$s) originates from A-triplet state formation, while the slow process ($w \sim$ ms) arises from transitions into the photo-oxidized radical state $\dot{R}^+$ of A. At similar I_{exc}, these transient state populations increase significantly with decreasing D−A distances.

For comparison, the corresponding D fluorescence ($\overline{F}_D$) for each D−A sample is plotted in red dots in Figure 7. $\overline{F}_D$ is approximately constant for $w \sim \mu$s and increases only slightly for the high FRET sample (10 Δbp). The slight increase in $\overline{F}_D$ suggests that the A-triplet state is less FRET-active than the A-singlet state, which would contradict the assumption made in eqs 2 and 3. One also has to consider that the increase in $\overline{F}_D$, resulting from D−A pairs, is diminished compared to the theoretically expected value due to a D-only labeled subfraction of DNA. Still, the increase in $\overline{F}_D$ is smaller than theoretically expected from the decrease in $\overline{F}_A$. To clarify how FRET-active the A-triplet state is, additional fluorescence cross-correlation experiments were performed. Given that the A-triplet state would be FRET-inactive, a transition of A into the triplet state would dequench and increase the D fluorescence while A becomes nonfluorescent. The resulting cross-correlation between the D and A fluorescence would show an anticorrelation in the time range of the A-triplet state. No such anticorrelation could be observed in the microsecond time range (data not shown). Hence, the A-triplet state is FRET-active, although supposedly with a slightly reduced efficiency compared to the $S^D_1 \rightarrow S^A_0$ efficiency. This finding thereby supports the approximation made in eq 2.

In addition to the electronic states depicted in Figure 1, a photo-oxidized radical state of D, $\dot{R}^{+D}$, is observed in the TRAST measurements (Figure 7). $\dot{R}^{+D}$ builds up for $w \sim$ ms and reduces the average $\overline{F}_D$. On the other hand, there is also a build-up of the A radical state $\dot{R}^{+A}$, which is FRET-inactive. This means that D cannot transfer energy to A any longer, and F_D is increased.

As can be seen in Figure 7, the influences of both phenomena on $\overline{F}_D$ largely cancel each other out. However, at low E, the first process slightly dominates, whereas at higher E, the effect of the R^{+A} build-up on $\overline{F}_D$ is more prominent.

The effect of A-transient states is much more prominent on the $\overline{F}_A$ curve than on the $\overline{F}_D$ curve (Figure 7). Thus, especially for low FRET efficiencies, $\overline{F}_A$ is more sensitive to FRET and hence more suitable as a read-out parameter for FRET determination by TRAST.

Determination of FRET Efficiencies. FRET efficiencies were calculated by fitting eqs 8 and 9 to the bleed-through corrected A fluorescence $\overline{F}_A(w)$. The thereby obtained $\overline{k}'_{ISC}$ is then used to calculate the FRET efficiency from eqs 3 and 4. In eqs 8 and 9, $\overline{k}'_{ISC}$, $\overline{k}'_{ox}$, and k_{red} are free fitting parameters, while the parameters k^A_{ISC}, k^A_T, $k^{D,A}_{10}$, and $\sigma^{D,A}_{exc,491}$ were kept constant for all samples. Here, k^A_{ISC} and k^A_T were determined from TRAST measurements of a D−A labeled reference sample (15 Δbp, $E = 0.4$) by fitting the measured fluorescence to eqs 8 and 9.

The obtained fits were in good agreement with the experimental data (Figure 7). The obtained redox rates ($k^A_{ox} \approx 1.4 \times 10^3\ s^{-1}$, $k_{red}{}^A \approx 0.5 \times 10^3\ s^{-1}$) were similar for all FRET samples. The FRET efficiencies computed from TRAST measurements were in good agreement with FRET efficiencies obtained from FCS and from the DNA model (Figure 6).

For the TRAST measurements, the error margins in Figure 6 were calculated by propagating the 95% confidence interval obtained by curve fitting eqs 8 and 9 to the computed $\overline{F}_A$ and by assuming 5% uncertainty in the laser power measurement.

4. FRET Efficiencies Determined by D Lifetime Measurements. For comparison, D lifetime measurements were also performed using time-correlated, single-photon counting, in the absence of KI and at optimal labeling conditions (for DA-samples, almost each D has an A). The D-only samples could be fitted with a single-exponential decay having a lifetime of 4.05 ± 0.01 ns. D lifetimes in the presence of A showed a multi-exponential decay behavior that could be fitted satisfactorily only with a two- to three-component lifetime model. One component with a decay time of $\tau_{F1} \sim 2.5$ ns was observed for all samples, while another component with a decay time of $\tau_{F2} \sim 4$ ns, corresponding to D-only labeled dsDNA, could only be distinguished from the FRET-reduced lifetimes (τ_{F3}) measured in D−A samples with Δbp < 24. Calculating E from τ_{F3} did not result in reasonable E values. Therefore, an average fluorescence lifetime was computed from τ_{F1} and τ_{F3} (from eq 11, and with $A_2 = 0$) and used for further FRET evaluations (eq 12). The resulting FRET efficiencies are plotted in Figure 6.

DISCUSSION

Our results suggest that, even in the presence of a large D-only labeled sample fraction, A-triplet state measurements can extend the useful range of intra- or intermolecular distances beyond the 10 nm limit[3,19,29,30] often stated for FRET-based methods. We have shown that FCS and TRAST measurements could unambiguously differentiate between samples of 0.4%, 3%, and 5% FRET efficiency, which corresponded to D−A distances of 14, 10, and 9 nm in this study. The presented approach monitors the triplet state build-up of the acceptor, which in turn depends on the FRET-mediated excitation of the dye. The general strategy of exploiting photoinduced, long-lived transient states of A was previously demonstrated by FRET-FCS measurements using the trans−cis isomerization kinetics of the cyanine dye Cy5 as a readout.[30] One advantage of exploiting the triplet state kinetics instead, as done in this study, is that this state is inherent to practically all organic fluorophores, which thus broadens the choice of available A dyes. In addition, because of an additional spectral correction used to compensate for D bleed-through, also FRET pairs with higher spectral overlap and possibly larger Förster radii can be applied. This should make it possible to observe D−A distances even beyond 15 nm. In this study, KI was used to suppress the D-triplet state and increase the sensitivity of the A-triplet state. The same effect can be obtained by using an A with a pronounced triplet state build-up.[31] In this case, the excitation intensities can be reduced to avoid a D-triplet state build-up. The resulting decreased molecular brightness of A is not an issue for the TRAST method as it can be compensated for by using higher concentrations or longer acquisition times.[14]

The results also predict that the technique is applicable to imaging using a standard laser scanning microscope or a wide-field microscope equipped with a time-modulated excitation. As a proof of principle, we have performed TRAST measurements in a one-point modus. The presented TRAST method showed that accurate FRET efficiencies could be calculated by modulating the excitation light in an on−off fashion using an AOM. However, the same kind of on−off modulation can also be obtained by scanning a laser beam over the sample and taking images with different scanning speeds, which result in different pixel dwell times.[16] Therefore, the same theory and data analysis that has been developed here can be applied for both TRAST concepts, independent of the experimental realization used.

Applying FCS for solution measurements or TRAST for FRET imaging has several advantages. We could show that, in the A-triplet state measurements, influences of D bleed-through and therefore also of D-only labeled subfractions can be fully corrected for. By the proposed correction procedure, D-only subpopulations as high as 99% could be tolerated when calculating the FRET efficiencies of the D−A samples. The influence of direct excitation of A in a D−A pair is included in the analysis. However, the influence of directly excited A-only labeled subfractions can only be disregarded as long as the direct excitation of A is negligible. In our measurements, a small fraction of A-only labeled samples did not change the FRET efficiency notably. However, for A-only fractions larger than 50%, we observed a moderate decrease in the apparent FRET efficiency.

In comparison, the corrections for spectral bleed-through in intensity-based FRET measurements are less robust.[2−5] Here, the FRET efficiencies are determined from the ratio of the fluorescence intensities detected in the A and in the D channel. The A−D intensity ratio has to be corrected for D bleed-through into the A channel and direct excitation of A. The D bleed-through can be determined from the ratio of the D fluorescence of a D-only labeled sample in the D and A channel. The extent of direct excitation of A is estimated by exciting A of an A-only labeled sample with the laser line used for FRET measurements and one suitable for direct excitation of A. However, the latter ratio will only be an estimate because the A intensity obtained by direct excitation might not be proportional to the A intensity obtained under different FRET conditions. For intensity-based FRET measurements, E will be an average of E from the D−A labeled subpopulation and the D-only labeled subpopulation with $E = 0$. Only an apparent, reduced E can be determined that will be dependent on the amount of D-only labeled samples. In this case, E can only be compared between different probes given

that the sample concentrations and labeling efficiencies are comparable from experiment to experiment.

In contrast, by A-triplet state measurements, one can suppress the influence of D-only labeled subpopulations by a simple reference measurement on the same sample. A D-only labeled reference sample is still required to determine the D-triplet state properties. However, the A-only labeled reference sample can be replaced with a sample of known FRET efficiency.

FRET lifetime measurements, on the other hand, have no constraints concerning spectral bleed-through. E is determined from the D fluorescence only, which, for appropriate filter conditions, will not be contaminated by the red-shifted A fluorescence. For the same reason, A fluorescence of directly excited A will not influence the D lifetime measurements. D lifetime measurements are able to distinguish D−A and D-only labeled sample fractions for high and intermediate E and reasonable D-only/D−A ratios. However, for lower E, the FRET-quenched D lifetime becomes comparable to the unquenched D lifetime, and the two components can not be properly separated. The resulting E will then be reduced compared to the actual D−A FRET efficiency. For high D-only/D−A ratios, the contribution of the quenched in relation to the unquenched D fluorescence will be minimal and difficult to distinguish in the data analysis.

The FRET D-lifetime measurements, presented in this study, were performed for optimal labeling conditions (ideally each D has an A). Given this, we were able to distinguish also low FRET efficiencies from each other (Figure 6). This would not have been possible for samples with a varying amount of D-only labeled subpopulations.

Interestingly, FCS, TRAST, as well as lifetime measurements underestimated the FRET efficiency of the high FRET sample (10 Δbp, $E_{model} = 0.95$). Strongly reduced FRET efficiencies for similar D−A distances have been reported before.[19] Possible reasons are (i) dimerization of D and A into a nonfluorescent complex, (ii) charge transfer between D−A through space interactions, or (iii) higher anisotropy values of D and A compared to the theoretical values used for random orientation of the fluorophores. Contrary to Dietrich et al.,[19] we did not observe dimerization (no shift in the absorption and emission spectra of the fluorophores bound to dsDNA). However, in the FCS measurements, we did observe a strongly reduced molecular brightness of A for the 10 Δbp sample in comparison to the 15 Δbp sample. This reduced molecular A brightness can, at least partially, be attributed to a strong bleaching of Alexa 610 due to the high FRET rate and simultaneous direct laser excitation. This is in analogy to a previous study,[29] where the photobleaching of red fluorophores was increased in the presence of a blue-shifted excitation outside of the excitation spectrum of the fluorophores. Hence, the population of higher excited states and consecutive bleaching from those states may be an underlying mechanism.

The multiexponential decay in our D lifetime measurements suggests additional energy transfer pathways from D to A, e.g., complex formation of the fluorophore with the base guanosine[32] or electron hopping via the guanosine bases of the DNA.[33,34] These processes would increase the apparent FRET efficiency, which is consistent with the FRET efficiencies determined from the D lifetime measurements in Figure 6. On the other hand, these additional processes can be included in the A-triplet state measurements, if k_{ISC}^{A} and k_{T}^{A} are determined on a D−A labeled reference sample with known FRET efficiency. At the same time, the influence of excitation saturation and bleaching artifacts on the FRET efficiency analysis is minimized.

Saturation and bleaching influence the determined k_{ISC}^{A} and k_{T}^{A} differently for FCS ($k_{ISC}^{A} = 2.1 \pm 0.1 \times 10^6\ s^{-1}$, $k_{T}^{A} = 0.2 \pm 0.01 \times 10^6\ s^{-1}$) and TRAST ($k_{ISC}^{A} = 3.6 \pm 0.13 \times 10^6\ s^{-1}$, $k_{T}^{A} = 0.14 \pm 0.01 \times 10^6\ s^{-1}$) measurements. For the applied excitation intensities in the upper range, FCS will tend to underestimate k_{ISC}^{A}.[22] This is reflected in the apparently decreased diffusion times observed in the correlation curves for higher excitation rates and indicates bleaching and thus depletion of singlet state fluorophores in the center of the focus. In TRAST, on the other hand, lower excitation intensities were used than for FCS. In addition, over the course of the whole pulse train a small fraction of A will bleach away that will be larger for longer pulse widths than for shorter pulse widths. As the diffusion of the DNA strands is quite slow, the bleached fluorophores will not totally renew within the off periods of the light modulation. This will lead to an apparently larger A-triplet fraction and therefore to an overestimation of k_{ISC}^{A}. To obtain absolute FRET efficiencies using FCS or TRAST, it is thus recommended to calibrate the A-triplet rates for a given FRET pair by using a reference sample with known FRET efficiency. Very often, however, only relative distances are to be measured, and these are very well reflected in the A-triplet state population without the need of an additional calibration step.

In conclusion, A-triplet state measurements provide a powerful tool to investigate long-range FRET efficiencies. Combined with a novel suppression algorithm for spectral bleed-through, the technique estimates accurately even low FRET efficiencies $\leq 5\%$, a FRET regime where donor lifetime or intensity based measurements are usually biased by D-only labeled specimen or by additional energy transfer processes. We predict that the approach will prove useful also on conventional laser scanning microscopes and wide-field microscopy settings.

AUTHOR INFORMATION

Corresponding Author

*E-mail: jerker@biomolphysics.kth.se. Phone: +46-8-5537 8030. Fax: +46-8-5537 8216.

Present Addresses

†Department of NanoBiophotonics, Max Planck Institute for Biophysical Chemistry, Göttingen, Germany.

ACKNOWLEDGMENT

This study was supported by means from EU FP7 (FLUODIAMON, 201 837) and the Swedish National Research Council (VR, 2009-3134). T.S. acknowledges funding from the "Fond national de la Recherche (Luxembourg)".

REFERENCES

(1) Förster, T. *Ann. Phys.* **1948**, *437*, 55–75.

(2) Gordon, G. W.; Berry, G.; Liang, X. H.; Levine, B.; Herman, B. *Biophys. J.* **1998**, *74*, 2702–2713.

(3) Beutler, M.; Makrogianneli, K.; Vermeij, R.; Keppler, M.; Ng, T.; Jovin, T.; Heintzmann, R. *Eur. Biophys. J.* **2008**, *38*, 69–82.

(4) Jovin, T. M.; Arndt-Jovin, D. J. *Annu. Rev. Biophys. Biophys. Chem.* **1989**, *18*, 271–308.

(5) Chen, Y.; Periasamy, A. *J. Fluoresc.* **2006**, *16*, 95–104.

(6) Ng, T.; Squire, A.; Hansra, G.; Bornancin, F.; Prevostel, C.; Hanby, A.; Harris, W.; Barnes, D.; Schmidt, S.; Mellor, H.; Bastiaens, P. I. n. H.; Parker, P. J. *Science* **1999**, *283*, 2085–2089.

(7) Eggeling, C.; Berger, S.; Brand, L.; Fries, J. R.; Schaffer, J.; Volkmer, A.; Seidel, C. A. M. *J. Biotechnol.* **2001**, *86*, 163–180.

(8) Sisamakis, E.; Valeri, A.; Kalinin, S.; Rothwell, P. J.; Seidel, C. A. M. Accurate Single-Molecule FRET Studies Using Multiparameter Fluorescence Detection Methods in Enzymology. In *Single Molecule Tools, Part B: Super-Resolution, Particle Tracking, Multiparameter, and Force Based Methods*; Walter, N. G., Ed.; Academic Press: New York, 2010; Vol. 475, p 455−514.
(9) Widengren, J.; Kudryavtsev, V.; Antonik, M.; Berger, S.; Gerken, M.; Seidel, C. A. M. *Anal. Chem.* **2006**, *78*, 2039–2050.
(10) Selvin, P. R. *Annu. Rev. Biophys. Biomol. Struct.* **2002**, *31*, 275–302.
(11) Selvin, P. R.; Hearst, J. E. *Proc. Natl. Acad. Sci. U.S.A.* **1994**, *91*, 10024–10028.
(12) Rajapakse, H. E.; Gahlaut, N.; Mohandessi, S.; Yu, D.; Turner, J. R.; Miller, L. W. *Proc. Natl. Acad. Sci. U.S.A.* **2010**, *107*, 13582–13587.
(13) Geissbuehler, M.; Spielmann, T.; Formey, A.; Marki, I.; Leutenegger, M.; Hinz, B.; Johnsson, K.; Van De Ville, D.; Lasser, T. *Biophys. J.* **2010**, *98*, 339–349.
(14) Sandén, T.; Persson, G.; Thyberg, P.; Blom, H.; Widengren, J. *Anal. Chem.* **2007**, *79*, 3330–3341.
(15) Spielmann, T.; Blom, H.; Geissbuehler, M.; Lasser, T.; Widengren, J. *J. Phys. Chem. B* **2010**, *114*, 4035–4046.
(16) Sandén, T.; Persson, G.; Widengren, J. *Anal. Chem.* **2008**, *80*, 9589–9596.
(17) Watson, J. D.; Crick, F. H. *Nature* **1953**, *171*, 737–738.
(18) Widengren, J.; Chmyrov, A.; Eggeling, C.; Löfdahl, P.-Å.; Seidel, C. *J. Phys. Chem. A* **2007**, *111*, 429–440.
(19) Dietrich, A.; Buschmann, V.; Müller, C.; Sauer, M. *Rev. Mol. Biotechnol.* **2002**, *82*, 211–231.
(20) Eggeling, C.; Widengren, J.; Rigler, R.; Seidel, C. A. M. *Anal. Chem.* **1998**, *70*, 2651–2659.
(21) Widengren, J.; Rigler, R. *Bioimaging* **1996**, *4*, 149–157.
(22) Widengren, J.; Mets, Ü.; Rigler, R. *J. Phys. Chem.* **1995**, *99*, 13368–13379.
(23) Widengren, J.; Rigler, R.; Mets, Ü. *J. Fluoresc.* **1994**, *4*, 255–258.
(24) Chmyrov, A.; Sandén, T.; Widengren, J. *J. Phys. Chem. B* **2010**, *114*, 11282–11291.
(25) Rigler, R.; Mets, U.; Widengren, J.; Kask, P. *Eur. Biophys. J.* **1993**, *22*, 169–175.
(26) Blom, H.; Chmyrov, A.; Hassler, K.; Davis, L. M.; Widengren, J. *J. Phys. Chem. A* **2009**, *113*, 5554–5566.
(27) Elson, E. L.; Magde, D. *Biopolymers* **1974**, *13*, 1–27.
(28) Widengren, J.; Seidel, C. A. M. *Phys. Chem. Chem. Phys.* **2000**, *2*, 3435–3441.
(29) Eggeling, C.; Widengren, J.; Brand, L.; Schaffer, J.; Felekyan, S.; Seidel, C. A. M. *J. Phys. Chem. A* **2006**, *110*, 2979–2995.
(30) Widengren, J.; Schweinberger, E.; Berger, S.; Seidel, C. A. M. *J. Phys. Chem. A* **2001**, *105*, 6851–6866.
(31) Chmyrov, A.; Arden-Jacob, J.; Zilles, A.; Drexhage, K.-H.; Widengren, J. *Photochem. Photobiol. Sci.* **2008**, *7*, 1378–1385.
(32) Eggeling, C.; Fries, J. R.; Brand, L.; Gunther, R.; Seidel, C. A. M. *Proc. Natl. Acad. Sci. U.S.A.* **1998**, *95*, 1556–1561.
(33) Jortner, J.; Bixon, M.; Langenbacher, T.; Michel-Beyerle, M. E. *Proc. Natl. Acad. Sci. U.S.A.* **1998**, *95*, 12759–12765.
(34) Giese, B. *Acc. Chem. Res.* **2000**, *33*, 631–636.